RESEARCH ARTICLE | SEPTEMBER 01 2023

Numerical thermo-mechanical study of elastic-plastic interaction of differently sized copper microparticles at high velocity FREE

Giedrius Jočbalis ✉; Rimantas Kačianauskas; Sergejus Borodinas; Jerzy Rojek

AIP Conf. Proc. 2849, 360001 (2023)
https://doi.org/10.1063/5.0162593

Numerical Thermo-Mechanical Study of Elastic-Plastic Interaction of Differently Sized Copper Microparticles at High Velocity

Giedrius Jočbalis[1, a)] Rimantas Kačianauskas[2, b)] Sergejus Borodinas[2, c)] and Jerzy Rojek[3, d)]

[1]*Antanas Gustaitis Aviation Institute, Vilnius Gediminas Technical University, Vilnius, Lithuania.*
[2]*Department of Applied Mechanics, Vilnius Gediminas Technical University, Vilnius, Lithuania.*
[3]*Institute of Fundamental Technological Research, Polish Academy of Sciences, Warsaw, Poland.*

[a)] Corresponding author: giedrius.jocbalis@vilniustech.lt
[b)] rimantas.kacianauskas@vilniustech.lt
[c)] sergejus.borodinas@vilniustech.lt
[d)] jerzy.rojek59@gmail.com

Abstract. High-velocity interaction between particles and nonflat surfaces is relevant to processes occurring in additive manufacturing technologies such as cold spray. The study of the behavior of the material during a high-velocity collision is needed to understand the full-scale process. The paper addresses the normal contact interaction between spherical particles as well as spherical surfaces at a velocity as high as 400 m/s. The problem is approached by numerical simulation applying the finite element method using strain, strain-rate, and temperature-dependent plasticity model. The focus of this report is to show the contribution of colliding particle radii to the interaction parameters. The results include contact duration, contact surface area, displacement, heat energy, stress, and strain rate.

INTRODUCTION

Cold spray is an additive manufacturing process in which the coating is formed by gradually depositing layers of particles using heat produced by plastic deformations of high-kinetic energy particles. The cold spray may use various metal powders for both the same and different material surface coatings.

In cold spray technology, particles impact rough substrate at very high velocity, causing near-melting or melting temperatures. In this paper, the substrate is considered as an extreme case of a particle with infinite or negative radius.

In plastic particle interaction, differently from laser-induced particle impact testing (LIPIT) [1], where only the substrate undergoes plastic deformation, the definition of characteristic strain rate hardening is not sufficient; therefore, a strain rate-sensitive plasticity model is used. A review of strain rate plasticity models can be found in [2]. The paper addresses the impact behavior of spherical particles and changes in the particle properties with high-velocity impact. The particular focus concerns the dependence of impact characteristics on the ratio of radii of the contact surfaces. These contributions are studied by applying the finite element method (FEM).

PROBLEM FORMULATION

Several cases of particle-to-particle normal collisions ranging from contact with smaller particles to contact with a concave surface (Figure 1) were modeled in a 2D axisymmetric plane. The smooth spherical particle of radius $R_1 = 20$ μm represents a typical size of the powder particles, colliding with particles of different sizes and curved substrates $R_2 = 10$, 20, 60, 100, 200, ∞ and -200 μm.

The motion of the particle in time is monitored by the average one-dimensional (1D) particle mass displacement d_{avg} and velocity v_{avg} of colliding particles in the normal direction. The impact begins with the initial relative velocity $v(t_0) = v_1(t_0) - v_2(t_0) = 400$ m/s. The particles undergo elastoplastic deformation and stop ($v(t) = 0$) reaching the maximum overlap depth $d = d_{max}$, then rebounds with rebound velocity $v_r(t)$.

International Conference of Numerical Analysis and Applied Mathematics ICNAAM 2021
AIP Conf. Proc. 2849, 360001-1–360001-4; https://doi.org/10.1063/5.0162593
Published by AIP Publishing. 978-0-7354-4589-5/$30.00

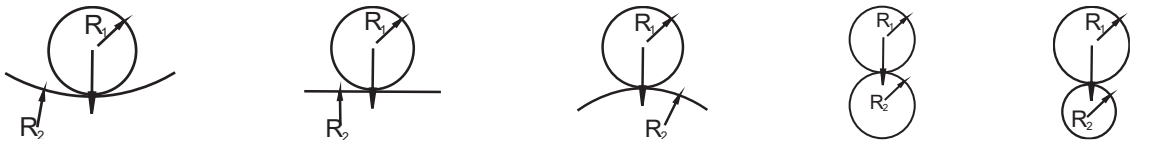

a) $R_1/R_2 < 0$ b) $R_1/R_2 = 0$ c) $0 < R_1/R_2 < 1$ d) $R_1/R_2 = 1$ e) $R_1/R_2 > 1$

FIGURE 1. Schematic illustration of impact: with a concave substrate (a), a flat substrate (b), a larger particle (c), a particle of the same size (d), and a smaller particle (e).

Mathematical Model

For the impact simulation of the particle-particle contact, non-linear coupled solid mechanics and heat transfer utilities of COMSOL Multiphysics FEA software was used. In this coupling, the heat transfer module is contributed by the dissipation power as a heat source while the solid mechanics module is contributed by the thermodynamic state of the material.

Material yielding point is defined by the combined state and time-dependent plasticity criterion (1) that allows separate evaluation of strain (described by Ludwik model [3]), strain-rate (described by Cowper-Symonds model [4]), and temperature (described by the Johnson-Cook model [5]) contributions.

$$\sigma_y(\varepsilon, \dot{\varepsilon}, T) = (A + B\varepsilon^n)\left(1 + D \cdot \left(\frac{\dot{\varepsilon}}{\dot{\varepsilon}_0}\right)^k\right)\left(1 - \left(\frac{T - T_r}{T_m - T_r}\right)^m\right), \quad (1)$$

The notation and values of the criterion constants are given in the material section.

Material

The material used for the simulation is taken as pure copper with Young's modulus E = 128 GPa, Poisson's ratio ν = 0.36, density ρ = 8960 kg/m^3, melting temperature T_m = 1085 K. Copper was chosen as a suitable material for the numerical simulation, as it is a material for which high strain-rate material data are available [1], [6]: initial yield stress A = 90 MPa, strength coefficient B = 292 Mpa, strain hardening exponent n = 0.31, strain-rate strengthening coefficient D = 0.19, strain-rate strengthening exponent k = 0.18, and thermal softening exponent m = 1.09 are Ludwik, Cowper-Symonds and Johnson-Cook plasticity criterion parameters used in Equation (1). Heating efficiency ratio a = 0.9 shows the fraction of dissipation power that is converted to heat energy.

NUMERICAL RESULTS AND DISCUSSION

To demonstrate the behavior of the particles with different radii, several cases of normal $R_1 = 20$ μm particle impact at a 400 m/s velocity were modeled. The ratio between contacting surface radii ranges from $-0.1 \leq R_1/R_2 \leq 2$. When a particle collides with a surface, collision kinetic energy equals particle kinetic energy, while in a collision between particles kinetic energy can be calculated as:

$$E_k = \frac{m_1 v_1^2 + m_2 v_2^2}{2} \quad (2)$$

Splitting the mass impulse equally ($m_1 v_1 = -m_2 v_2$) between particles

$$v_i = \pm v R_j^3 / (R_i^3 + R_j^3) \quad (3)$$

Adding (3) and the definition of sphere mass to (2), the kinetic energy can be written as:

$$E_k = \pi \rho v \frac{2R_1^3 R_2^3}{3(R_1^3 + R_2^3)} \quad (4)$$

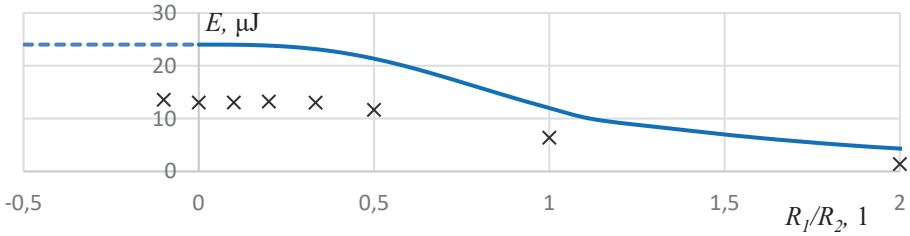

FIGURE 2. Energy in contact as a function of the ratio of contacting surface radii.

The dependency of kinetic energy on the ratio of the radii of the contact surfaces is shown in Figure 2, with the heat energy after the collision of several modeled cases added for comparison. As we can see from Figure 2, the kinetic energy reduces in particle-particle contact. The dashed line shows the particle to concave surface cases, x represents the system heat energy after the collision.

The results of the characteristic cases will be presented in figures 3–6. The end of the loading stage (maximum displacement) is characterized by velocity $v_{avg} = 0$, and the end of the contact stage (rebound) by contact area $a_c = 0$. The distribution of the strain rate in the particle is complicated, so it is also characterized by the average value $\dot{\varepsilon}_{avg}$. Characteristic strain rate for case $R_2 = \infty$ is usually considered as

$$\dot{\varepsilon}_{ch} = \frac{v}{2R_1} = 10^7 \text{ s}^{-1}, \quad (5)$$

The difference in contact duration between different cases of the contact surface can be seen in Figure 3.

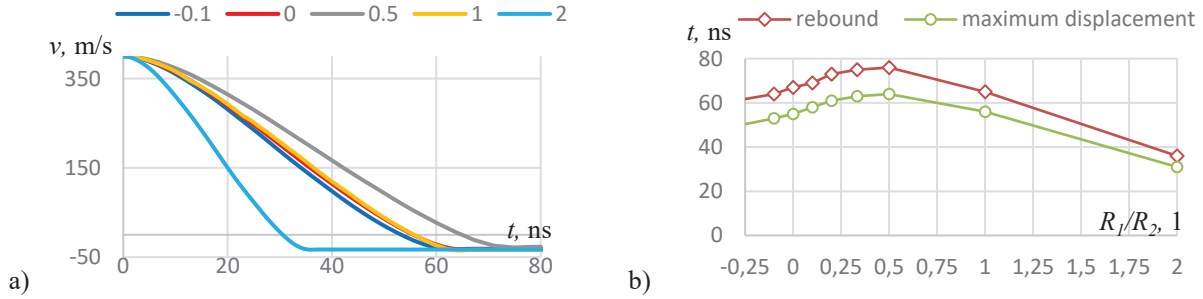

FIGURE 3. Results for different contact surface radii: particle relative velocity (a), loading stage, and contact stage duration (b)

In Figure 3, we see that both loading and contact duration are the longest for the impact on the particle with double the original size ($R_1/R_2 = 0.5$). The cases are further investigated in Figure 4.

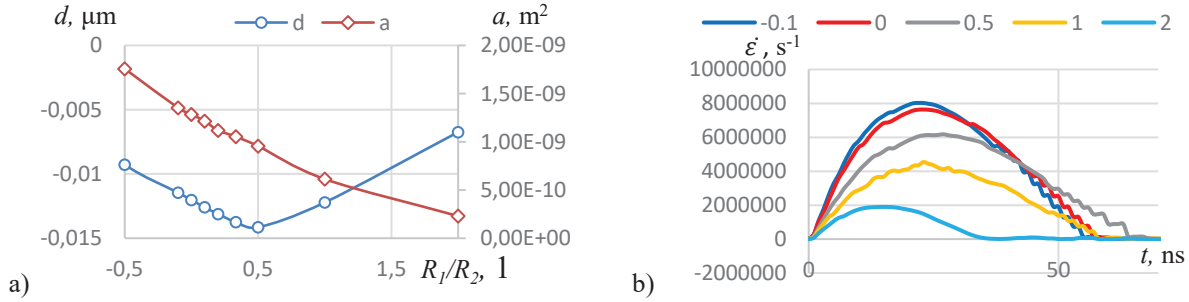

FIGURE 4. Results for different contact surface radii: particle relative maximum displacement d and maximum contact area a (a) average strain-rate of $R_1 = 20$ μm particle (b)

In Figure 4a, we see that the particle contact duration corresponds to the maximum relative displacement. Figure 4b shows the average strain rate in all cases lower than the characteristic value. The distribution of stress at the time of maximum average strain rate is shown in Figure 5.

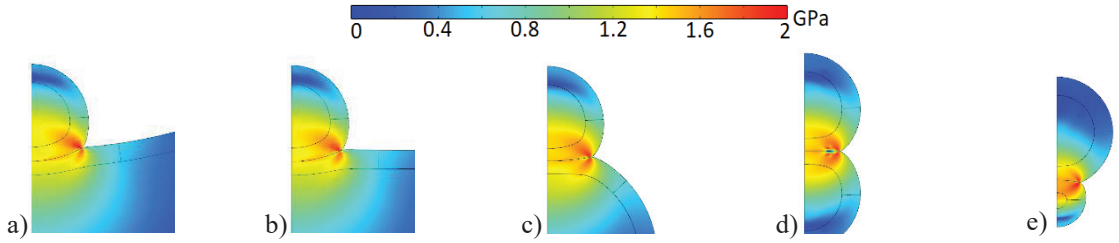

FIGURE 5. Illustration of von-Misses stress at the time of the highest average strain rate during impact with a concave substrate (a), a flat substrate (b), a larger particle (c), a particle of the same size (d) and a smaller particle (e).

From Figure 5, we see that higher stress values, as well as higher strain and strain rates, occur in particles with a smaller radius. The temperature at the time instance of rebound is shown in Figure 6.

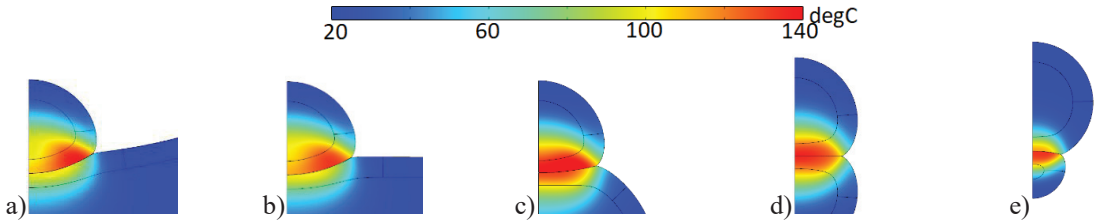

FIGURE 6. Illustration of temperature at time instance of rebound: impact on a concave substrate (a), a flat substrate (b), larger particle (c), a particle of the same size (d), and smaller particles (e)

As we can see in Figure 6, the smaller particle gains higher temperature during impact. The range of temperatures is similar between all tested cases. Maximum temperatures during contact range from 134.8 °C to 150.5 °C with the case of $R_1/R_2 = 0.5$ having the highest temperature.

CONCLUSIONS

To investigate the contribution of the ratio of contacting radii, particle contact at a 400 m/s relative velocity was modeled. The following conclusions were drawn:

The contact partner with a smaller radius undergoes greater stress, strain, and strain rate. Therefore, it generates more heat energy as a result of plastic dissipation. However, the average strain rate is lower than the calculated characteristic strain rate.

Contact area decreases with contacting radius getting smaller and increases in contact with a concave surface. Participating kinetic energy is lower in particle-to-particle contact. Due to these facts, the contact duration, maximum relative displacement, and temperature peaks at $R_1/R_2 = 0.5$ value. The contact surface at this value is still relatively small, and the kinetic energy of the contact is high.

The duration of the loading phase amounts to 80-86% of the contact duration and is higher with an increase in the value R1 / R2.

ACKNOWLEDGEMENTS

This work was supported by the Research Council of Lithuania under project No. S-MIP-19-25.

REFERENCES

[1] M. Hassani, D. Veysset, K.A. Nelson, C.A. Schuh, Material hardness at strain rates beyond 106 s−1 via high velocity microparticle impact indentation, Scr. Mater. 177 (2020) 198–202. https://doi.org/10.1016/j.scriptamat.2019.10.032.

[2] A. Hor, F. Morel, J. Lou Lebrun, G. Germain, Modelling, identification and application of phenomenological constitutive laws over a large strain rate and temperature range, Mech. Mater. 64 (2013) 91–110. https://doi.org/10.1016/j.mechmat.2013.05.002.

[3] P. Ludwik, Elemente der Technologischen Mechanik, Springer Berlin Heidelberg, Berlin, Heidelberg, 1909. https://doi.org/10.1007/978-3-662-40293-1.

[4] G. Cowper, P. Symonds, Technical report (Brown University. Division of Applied Mathematics), Strain-hardening and strain-rate effects in the impact loading of cantilever beams, 1957. https://doi.org/10.21236/AD0144762.

[5] G.R. Johnson, W.H. Cook, Fracture characteristics of three metals subjected to various strains, strain rates, temperatures and pressures, Eng. Fract. Mech. 21 (1985) 31–48. https://doi.org/10.1016/0013-7944(85)90052-9.

[6] M.R.W. Brake, P.L. Reu, D.S. Aragon, A Comprehensive Set of Impact Data for Common Aerospace Metals, J. Comput. Nonlinear Dyn. 12 (2017) 1–23. https://doi.org/10.1115/1.4036760.